Quantification of microscale factors for fatigue failure in NiTi shape memory alloys

Xiaofei Ju, Ziad Moumni, András Borbély, Yahui Zhang, Shengyi Zhong

Journal of Materials Research and Technology 31 (2024) 1–5

Contents lists available at ScienceDirect

Journal of Materials Research and Technology

journal homepage: www.elsevier.com/locate/jmrt

Quantification of microscale factors for fatigue failure in NiTi shape memory alloys

Xiaofei Ju [a], Ziad Moumni [a,*], András Borbély [b], Yahui Zhang [c], Shengyi Zhong [d]

[a] UME, ENSTA-Paris, Institut Polytechnique de Paris, 91120 Palaiseau, France
[b] Mines Saint-Etienne, Université de Lyon, CNRS, UMR 5307 LGF, F-42023, Saint-Étienne, France
[c] State IJR Center of Aerospace Design and Additive Manufacturing, Northwestern Polytechnical University, 710072 Xi'an, China
[d] School of Materials Science and Engineering, Shanghai Jiao Tong University, Shanghai, 200240, China

ARTICLE INFO

Keywords:
Shape memory alloys (SMAs)
X-ray diffraction (XRD)
Fatigue
Microstructure quantification
Stored energy

ABSTRACT

Fatigue behavior is intrinsically linked to microstructural alterations induced by cyclic loading. However, the quantification of microstructural defects associated with fatigue damage of NiTi shape memory alloys (SMAs) is lacking, which hinders the development of a physically based fatigue criterion. To this end, a multi-scale experimental analysis was conducted on cyclically deformed NiTi SMAs, which evidenced a strong correlation between microstructural inhomogeneity and localized deformation behavior. The microstructural change associated with fatigue was quantified in terms of stored strain–energy, with the highest values observed in the regions where fatigue cracks initiate. Consequently, stored energy is deemed as an effective fatigue indicator, offering valuable insights for future work in the design and optimization of SMAs' structures against fatigue.

Pseudoelastic shape memory alloys (SMAs) are widely used in various industrial fields owing to their unique property of large inelastic strain recovery, with their fatigue behavior being an essential concern [1–3]. Fatigue failure, marked by crack initiation and growth, is intricately linked to microstructural evolution during cyclic loading [4–8], necessitating the incorporation of this information into fatigue analysis. This is particularly crucial for pseudoelastic NiTi SMAs, characterized by inhomogeneous deformation that leads to significant discrepancies between global and local behavior [9–11], and preferential fatigue failure in specific regions known as active zones [12,13]. The existing fatigue criteria for SMAs are mainly empirical and based on macroscopic parameters such as stress, strain, and dissipated energy [14–18]. Although some studies have suggested using local strain instead of global strain to better represent the effects of localized deformation [11,13], these parameters are still fundamentally macroscopic. Consequently, current fatigue criteria do not adequately capture the intrinsic physical mechanisms of fatigue at microscale, thereby failing to fully reflect the impact of localized deformation on fatigue behavior. To establish a physically-based fatigue criterion that incorporates microstructural changes, there is a clear necessity for their quantification. While extensive research has been conducted experimentally at microscale to explore the impact of initial microstructures (including TiC inclusions, precipitates, processing defects and grain size) [19–22] and varying inelastic mechanisms (phase transformation and its associated plastic deformation) [5,23–25,25–33] on fatigue, a quantitative analysis of specifically addressing the overall impact of these factors within the context of fatigue behavior in SMAs is still lacking.

Against this background, a combined use of Digital Image Correlation (DIC), high-resolution X-ray diffraction (XRD) and Transmission Electron Microscopy (TEM) is proposed in the present work to conduct a quantitative analysis on the cyclically loaded NiTi SMAs. Global microstructural changes due to inhomogeneous deformation are identified and quantified via X-ray line-profile analysis (XLPA) in terms of stored energy. Stored energy is used in the present work as the quantity accounting for the microstructural evolution during fatigue, which is intrinsically associated with the strain field of the generated crystal defects. While recognized as a robust fatigue indicator in elasto-plastic materials [34–36], stored energy has received little attention in the domain of SMAs [37]. Notably, our finding reveals that stored energy is the highest in the active zones, which are the preferential sites for damage in SMAs [12,13]. This work provides a methodology to quantify the microstructural changes and lays the foundation for an improved fatigue criterion for SMAs.

Pseudoelastic polycrystalline Ti-55.85 wt.% Ni strips (Johnson Matthey Inc., USA) with the austenite finish temperature $A_f \approx 6$ °C were used. The fatigue behavior of NiTi SMAs utilized in this study has been

* Corresponding author.
E-mail address: ziad.moumni@ensta-paris.fr (Z. Moumni).

https://doi.org/10.1016/j.jmrt.2024.05.260
Received 16 March 2024; Accepted 30 May 2024
Available online 1 June 2024

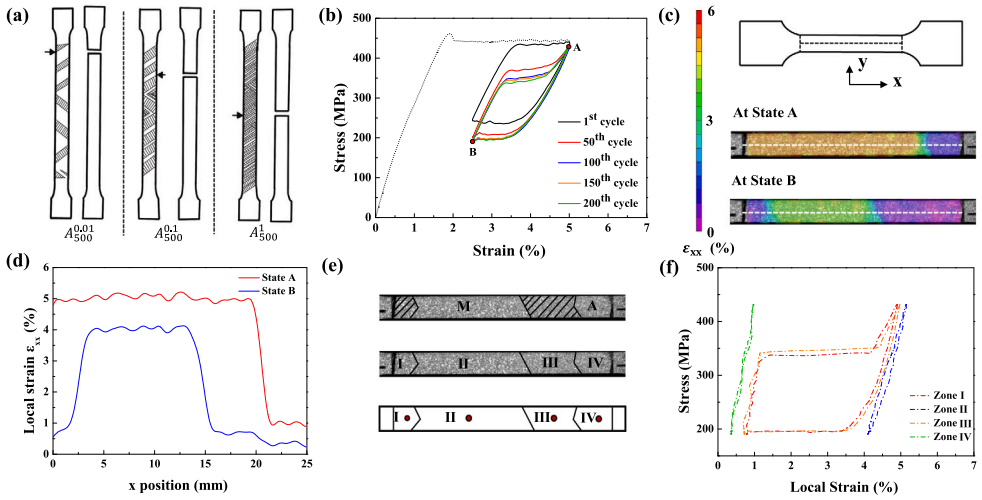

Fig. 1. (a) Fatigue results of a series of NiTi strips under different loading conditions obtianed by Zheng et al. [13]. Transformation patterns (shaded areas indicate active zones) and fatigue failure points (arrows) are shown. Label $A_{500}^{0.01}$ represents specimen A tested under $\sigma_{max} = 500$ MPa and $f = 0.01$ Hz; (b) Nominal stress–strain curves of cyclic loading; (c) The DIC strain maps in states A and B at cycle 200; (d) The corresponding strain distribution along the centerline of the gauge section; (e) Different zones marked on the optical and schematic maps. The red points at the center of the zones represent the positions where the local stress–strain curves shown in Fig. 1(f) were measured. (For interpretation of the references to color in this figure legend, the reader is referred to the web version of this article.)

systematically investigated in a prior work by Zheng et al. [12,13], unveiling an inhomogeneous deformation characterized by transformation patterns and preferential failure within specific zones as evidenced in Fig. 1(a). Based on these established findings, current investigation follows their experimental method, focusing on a single specimen subjected to cyclic deformation. The objective is to identify and quantify the microstructural alterations and to explore their correlations with preferential fatigue failure. A strain-control mode at a low loading rate was chosen in order to simplify the transformation patterns [12]. The corresponding stress–strain curve is shown in Fig. 1(b). The specimens reached steady state after 100 cycles; hence, samples subjected to 200 cycles were chosen as a study subject for further microstructural analysis. The morphology of the samples' surface was synchronously monitotred by a CMOS camera with 2048 × 1088 pixels. The local strain field was obtained from the optical images processed with the DIC software Vic-2D. Further insight into the inhomogeneous deformation in terms of microstructural changes was obtained by XLPA and TEM. The diffraction profiles were measured with a Panalytical MRD diffractometer equipped with hybrid monochromator (2 × Ge220 crystals and a parabolic mirror) and a linear position sensitive detector. The instrumental broadening was negligible compared to the physical broadening of the specimens. TEM observations were carried out using FEI TITAN Themis 300 operated at 300 kV.

Figs. 1(c)–(f) show the DIC results of the NiTi strips at cycle 200. The inhomogeneous deformation is evident from the local strain maps depicted in Figs. 1(c) and (d). At the maximum nominal strain (state A), most regions are in the high-strain level (with a local strain of 5%) and mostly contain stress-induced martensite. A small region showing a low-strain level (with a local strain of 1%) remains austenite [29]. At the minimum nominal strain (state B), part of the high-strain region changes to low-strain level indicating reverse phase transformation. Such region experiences cyclic phase transformation and is marked as active zone. In contrast, other regions remain in relatively high-strain level and contain untransformed martensite. Based on this features the gauge section can be divided into several zones [12]: the active zones (shaded with lines), the martensite zone (M) and the austenite zone (A), as shown in Fig. 1(e) (marked by I–IV). To elucidate the local strain evolution during one cycle, the values corresponding to the zone centers (marked by red points) were plotted against the nominal stress in Fig. 1(f). It can be seen that zone I and III show similar pseudoelastic behavior, indicating a cycle of forward and reverse phase transformation occurring in the active zones. The curves for zones II and IV indicate a nearly "elastic" deformation taking place in the M and A domains [13].

High-resolution XRD peaks were acquired from both the as-received and cyclically deformed samples (Fig. 2). The diffractogram of the as-received sample (Fig. 2(a)) confirms the presence of only austenite with no evidence of martensite. The comparison of the 222 peaks measured at the center of zones I–IV in the deformed sample is shown in Fig. 2(b). The 222 peak shapes (including the widths and tails) for zones II and IV are almost identical to that of the as-received sample, while the peaks for zones I and III are broader. In addition to peak broadening, a peak shift towards higher 2θ angles in the actives zones I and III is also observed. According to [25,38], this peak shift could originate from the accumulation of residual martensite and residual stresses upon cyclic transformation. We further plot the peak width and lattice plane distance d_{222} as a function of the position from the left end of the sample in Figs. 2(c) and (d). Consistent with Fig. 2(b), larger peak width (characterized by the full width half maximum FWHM) and smaller d are observed in the active zones (zone I and III) compared to the other two. The observed variation delineates distinct zones, aligned closely with those identified by DIC. This suggests that the global microstructural inhomogeneity is efficiently captured by XRD, and the correlation between this inhomogeneity and localized deformation behavior is evident.

The inhomogeneous microstructures associated with localized deformation were further characterized at a lower scale by TEM (Fig. 3). Compared to the as-received sample, the martensite zone shows similar microstructure, while obvious distinctions are discernible in the active zone. This observation is in line with the XRD results, where the peak shapes for the M domain and for the as-received state are identical, while significant differences are found for the peaks of active zones (Fig. 2(b)). As shown in (Fig. 3(h)), a weak reflection, marked as TBD (to be determined), is observed in the active zone. Based on calculations, this reflection is not associated with austenite but likely corresponds to either to martensite or to the R-phase. However, due to the uncertainties inherent in measurement and calculation, as well as the variations in theoretical values attributable to atomic composition, it is challenging to conclusively determine through TEM whether the reflection belongs to the martensite or to the R-phase. It is noteworthy that no analogous undetermined diffraction spots were present in either the as-received sample or in the martensite zone. This observation suggests that the presence of residual martensite or R-phase is a unique

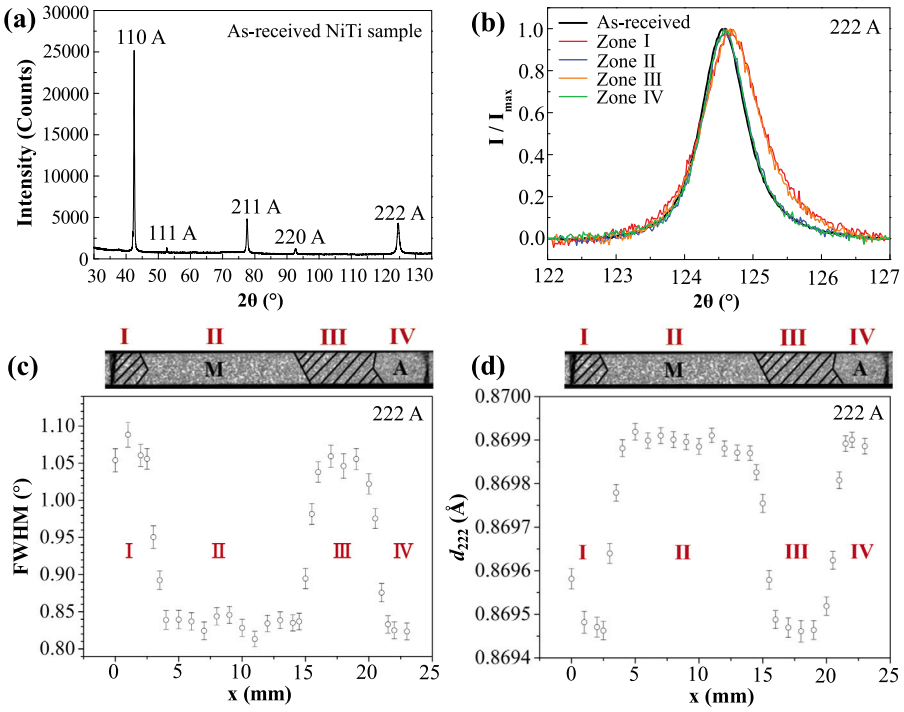

Fig. 2. (a) X-ray diffraction pattern of the as-received NiTi sample; (b) 222 bragg peaks of the B2 phase measured on the as-received and in different zones of the deformed sample (with background subtracted); FWHM (c) and the lattice plane distance (d) variation of the 222 peaks, as a function of the distance from the left end of the sample. The d-spacing was measured in the direction perpendicular to the sample surface and to the applied load, which is horizontal in Fig. 1(c). (For interpretation of the references to color in this figure legend, the reader is referred to the web version of this article.)

feature of the active zone in the deformed sample. Besides, deformation bands are also present exclusively in the active zone, which are associated with the localization of the irrecoverable strain (Fig. 3(i)).

Notable differences in the microstructure of the active zones, in comparison with that of the other two regions and the as-received state, are indicated by XRD and TEM analyses. These observations align with the findings presented in [9,10,39], which suggest that damage is influenced by local mechanisms related to inhomogeneous deformation during cycling. Building on these observations, subsequent work attempts to quantify microstructural changes that are potentially linked to fatigue failure. Peak broadening was described according to the Williamson–Hall model [40] in terms of size and microstrain effects:

$$\Delta K = 0.9/D + \varepsilon K, \tag{1}$$

where $\Delta K = 2\cos\theta(\Delta\theta)/\lambda$ represents the FWHM of the peaks in the reciprocal space, D is the crystallite size, $K = 2\sin\theta/\lambda$ is the scattering vector and λ the wavelength of the X-rays. ε is the microstrain (also called root-mean-square strain), associated to the standard deviation of the relative inter-planar spacing distribution [41,42]. Given the beam size of $\sim$ 150 μm × 50 μm for labo-XRD setup, the microstrain measured at the micrometer scale is summed up over a mesoscopic region. Therefore, this quantity might be considered as a "bridging" parameter between microscale and macroscale. Fig. 4 shows the FWHM of 3 reflections of the as-received and deformed samples as a function of K. The microstrain in the as-received sample is identical to that in the martensite zone (zone II) ($\varepsilon = (20 \pm 7) \times 10^{-4}$) while a larger value was found in the active zone (zone III) ($\varepsilon = (34 \pm 2) \times 10^{-4}$). The microstrain can be further used for the calculation of stored energy based on the model of Faulkner (Eq. (6b) in [43]). Consistent with microstrain observations, a higher stored energy is revealed in the active zone ($E_{st} = (1.04 \pm 0.12)$ MJ/m^3) than in the as-received sample or in the martensite zone ($E_{st} = (0.4 \pm 0.25)$ MJ/m^3). The stored energy resides within the field surrounding lattice defects and increases with defect density. Ultimately, it has the potential to induce crack formation upon reaching a critical value. Given the microstructural inhomogeneity identified by XRD and TEM analyses, the variation in stored energy across different regions indicates its capability in quantifying such inhomogeneity. Notably, highest magnitudes of stored energy are found to correlate with the regions more susceptible to fatigue cracking (active zones), suggesting the feasibility of using the stored energy as an effective indicator for fatigue in SMAs (see Fig. 4).

It is crucial to recognize that the current estimation of stored energy is based on average values across mesoscopic regions, effectively capturing the effects of global microstructural changes but possibly overlooking local inhomogeneities at nano-scale. Initial defects such as TiC inclusions and precipitates play a critical role in fatigue processes and are often the primary sources of failure. These defects can cause localized accumulations of stored energy that alter fatigue behavior. Specifically, TiC inclusions in NiTi create stress concentrations and initiate cracks during fatigue experiments [19,20], while small coherent precipitates can significantly influence fatigue by enhancing dislocation activity [22]. To capture the local effect of these initial defects and precisely correlate local stored energy with specific sites of fatigue crack initiation — rather than a broad region — employing high spatial-resolution measurements, such as microbeams at synchrotron sources, is essential. Building on this approach, a quantitative relationship between local stored energy and fatigue lifetime of SMAs could be determined through a series of measurements. In contrast to previous fatigue criteria, this approach enables the identification of positions susceptible to preferential fatigue failure, as marked by the peak of local stored energy. Furthermore, the local stored energy could be computed using finite element simulations, which is of great importance for the design and optimization of SMAs' structures to enhance fatigue resistance.

In summary, a multi-scale experimental analysis was conducted to investigate the localized deformation behavior of pseudoelastic NiTi SMAs, with an emphasis on quantifying the microstructural change linked to fatigue. By using XRD and TEM, the microstructural inhomogeneity was identified and demonstrated a significant correlation

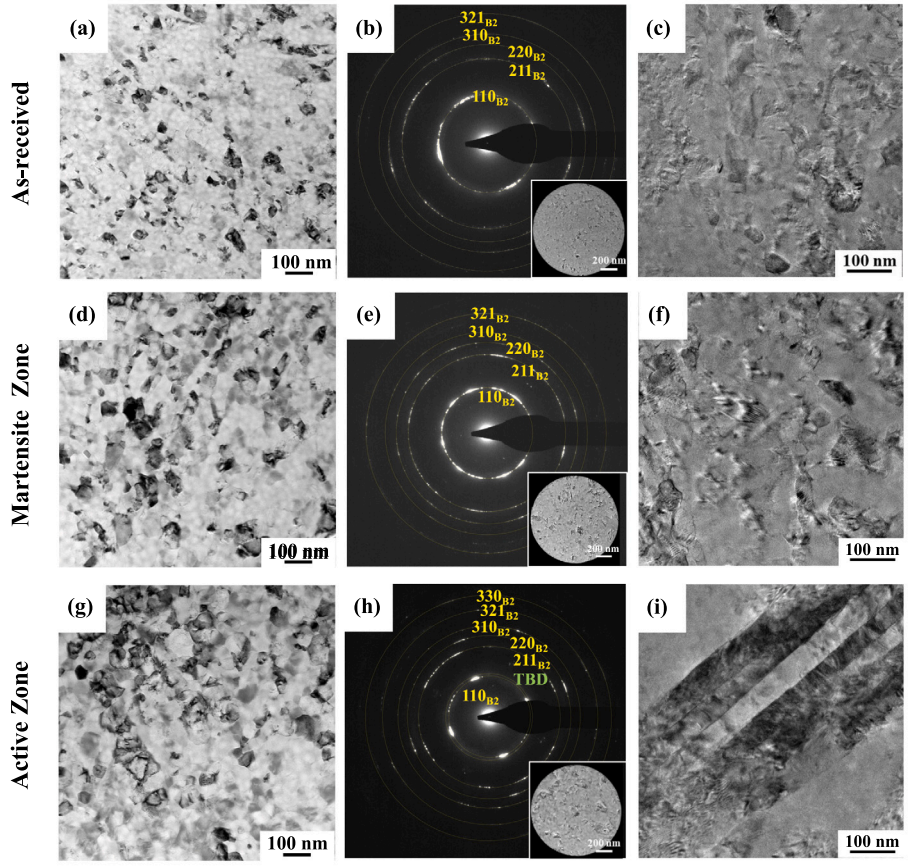

Fig. 3. TEM results showing bright-field images, selected-area diffraction patterns (SADPs) and microstructural images of the as-received NiTi sample (a–c); the martensite zone (d–f) and the active zone (g–i) of the deformed sample as marked in Fig. 1(e), respectively. For the diffraction ring whose phase identification is uncertain, the corresponding indice is marked as TBD (to be determined) on the pattern.

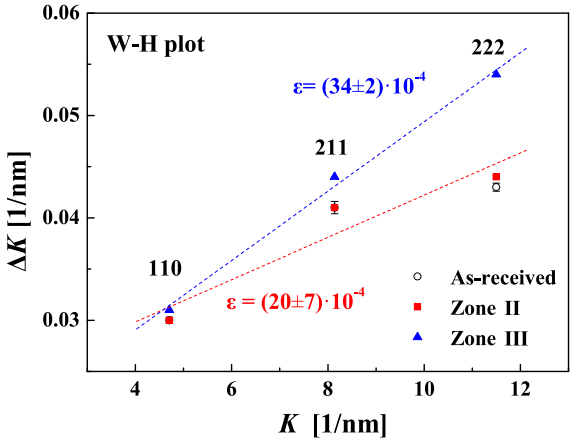

Fig. 4. Williamson–Hall plot of the austenite 110, 211 and 222 peak measured on the as-received and deformed sample. The hollow circle represents the data for as-received NiTi sample. The red square and blue triangle represent the data for zones II (martensite zone) and III (active zone) marked in Fig. 1(e). (For interpretation of the references to color in this figure legend, the reader is referred to the web version of this article.)

with localized deformation behavior detected by DIC method. The study quantified the microstructural changes in terms of stored energy, revealing that regions exhibiting the highest stored energy directly align with those where fatigue cracks are reported to occur. This work proposes a method for quantifying the global microstructural changes via stored energy, and demonstrates the potential of stored energy as a indicator for fatigue assessment in SMAs.

Declaration of competing interest

The authors declare that they have no known competing financial interests or personal relationships that could have appeared to influence the work reported in this paper.

References

[1] Patoor Etienne, Lagoudas Dimitris C, Entchev Pavlin B, Brinson L Catherine, Gao Xiujie. Shape memory alloys, Part I: General properties and modeling of single crystals. Mech Mater 2006;38(5–6):391–429.
[2] Jani Jaronie Mohd, Leary Martin, Subic Aleksandar, Gibson Mark A. A review of shape memory alloy research, applications and opportunities. Mater Des (1980-2015) 2014;56:1078–113.
[3] Luo Junfeng, Xu Guojin, Zhang Qiaoxia, Li Yongjun, He Jinjiang. Deformation mechanisms of a NiTi alloy under high cycle fatigue. J Mater Res Technol 2022;21:2693–703.
[4] Rahim M, Frenzel J, Frotscher M, Pfetzing-Micklich J, Steegmüller R, Wohlschlögel M, et al. Impurity levels and fatigue lives of pseudoelastic NiTi shape memory alloys. Acta Mater 2013;61(10):3667–86.
[5] Gloanec Anne-Lise, Bilotta Giovambattista, Gerland Michel. Deformation mechanisms in a TiNi shape memory alloy during cyclic loading. Mater Sci Eng A 2013;564:351–8.
[6] Hua Peng, Chu Kangjie, Ren Fuzeng, Sun Qingping. Cyclic phase transformation behavior of nanocrystalline NiTi at microscale. Acta Mater 2020;185:507–17.
[7] Chu Kangjie, Sun Qingping. Reducing functional fatigue, transition stress and hysteresis of niti micropillars by one-step overstressed plastic deformation. Scr Mater 2021;201:113958.
[8] Ge Jinguo, Yuan Bo, Zhao Lun, Yan Ming, Chen Wei, Zhang Liang. Effect of volume energy density on selective laser melting NiTi shape memory alloys: microstructural evolution, mechanical and functional properties. J Mater Res Technol 2022;20:2872–88.
[9] Alarcon Eduardo, Heller Luděk, Chirani Shabnam Arbab, Šittner Petr, Kopeček Jaromír, Saint-Sulpice Luc, et al. Fatigue performance of superelastic NiTi near stress-induced martensitic transformation. Int J Fatigue 2017;95:76–89.

[10] Furgiuele Franco, Magarò Pietro, Maletta Carmine, Sgambitterra Emanuele. Functional and structural fatigue of pseudoelastic NiTi: global vs local thermo-mechanical response. Shap Mem Superelasticity 2020;6:242–55.
[11] Sgambitterra Emanuele, Magarò Pietro, Niccoli Fabrizio, Renzo Danilo, Maletta Carmine. Novel insight into the strain-life fatigue properties of pseudoelastic NiTi shape memory alloys. Smart Mater Struct 2019;28(10):10LT03.
[12] Zheng Lin, He Yongjun, Moumni Ziad. Lüders-like band front motion and fatigue life of pseudoelastic polycrystalline NiTi shape memory alloy. Scr Mater 2016;123:46–50.
[13] Zheng Lin, He Yongjun, Moumni Ziad. Investigation on fatigue behaviors of NiTi polycrystalline strips under stress-controlled tension via in-situ macro-band observation. Int J Plast 2017;90:116–45.
[14] Song Di, Kang Guozheng, Kan Qianhua, Yu Chao, Zhang Chuanzeng. Damage-based life prediction model for uniaxial low-cycle stress fatigue of super-elastic NiTi shape memory alloy microtubes. Smart Mater Struct 2015;24(8):085007.
[15] Maletta Carmine, Sgambitterra E, Furgiuele Franco, Casati Riccardo, Tuissi A. Fatigue of pseudoelastic NiTi within the stress-induced transformation regime: a modified Coffin–Manson approach. Smart Mater Struct 2012;21(11):112001.
[16] Moumni Z, Van Herpen A, Riberty P. Fatigue analysis of shape memory alloys: energy approach. Smart Mater Struct 2005;14(5):S287.
[17] Runciman Amanda, Xu David, Pelton Alan R, Ritchie Robert O. An equivalent strain/Coffin–Manson approach to multiaxial fatigue and life prediction in superelastic Nitinol medical devices. Biomaterials 2011;32(22):4987–93.
[18] Kan Qianhua, Kang Guozheng, Yan Wenyi, Dong Yawei, Yu Chao. An energy-based fatigue failure model for super-elastic NiTi alloys under pure mechanical cyclic loading. In: Third international conference on smart materials and nanotechnology in engineering, vol. 8409. SPIE; 2012, p. 129–36.
[19] Tyc Ondřej, Molnarova Orsolya, Šittner Petr. Effect of microstructure on fatigue of superelastic NiTi wires. Int J Fatigue 2021;152:106400.
[20] Sawaguchi Tak Ahiro, Kausträter Gregor, Yawny Alejandro, Wagner Martin, Eggeler Gunther. Crack initiation and propagation in 50.9 at. pct Ni-Ti pseudoelastic shape-memory wires in bending-rotation fatigue. Metall Mater Trans A 2003;34:2847–60.
[21] Wang XM, Wang YF, Yue ZF. Finite element simulation of the influence of TiC inclusions on the fatigue behavior of NiTi shape-memory alloys. Metall Mater Trans A 2005;36:2615–20.
[22] Gall Ken, Maier HJ. Cyclic deformation mechanisms in precipitated NiTi shape memory alloys. Acta Mater 2002;50(18):4643–57.
[23] Eggeler Gg, Hornbogen E, Yawny A, Heckmann A, Wagner M. Structural and functional fatigue of NiTi shape memory alloys. Mater Sci Eng A 2004;378(1–2):24–33.
[24] Delville R, Malard B, Pilch J, Sittner P, Schryvers D. Transmission electron microscopy investigation of dislocation slip during superelastic cycling of Ni–Ti wires. Int J Plast 2011;27(2):282–97.
[25] Sedmák P, Šittner P, Pilch J, Curfs C. Instability of cyclic superelastic deformation of NiTi investigated by synchrotron X-ray diffraction. Acta Mater 2015;94:257–70.
[26] Heller L, Seiner H, Šittner P, Sedlák P, Tyc O, Kadeřávek L. On the plastic deformation accompanying cyclic martensitic transformation in thermomechanically loaded NiTi. Int J Plast 2018;111:53–71.
[27] Hurley Jay, Ortega Alicia M, Lechniak Jason, Gall Ken, Maier Hans J. Structural evolution during the cycling of NiTi shape memory alloys. Int J Mater Res 2022;94(5):547–52.
[28] Gao Pengyue, Li Runguang, Liu Yuzi, Chen Guangyao, Zhu Ming, Jian Yongxin, et al. In-situ synchrotron diffraction study of the localized phase transformation and deformation behavior in NiTi SMA. Mater Sci Eng A 2021;805:140560.
[29] Brinson L Catherine, Schmidt Ina, Lammering Rolf. Stress-induced transformation behavior of a polycrystalline NiTi shape memory alloy: micro and macromechanical investigations via in situ optical microscopy. J Mech Phys Solids 2004;52(7):1549–71.
[30] Kang Guozheng, Kan Qianhua, Qian Linmao, Liu Yujie. Ratchetting deformation of super-elastic and shape-memory NiTi alloys. Mech Mater 2009;41(2):139–53.
[31] Chowdhury Piyas, Sehitoglu Huseyin. A revisit to atomistic rationale for slip in shape memory alloys. Prog Mater Sci 2017;85:1–42.
[32] Zhang Yahui, Li Weichen, Moumni Ziad, Zhu Jihong, Zhang Weihong, Zhong Sheng-Yi. Degradation of the recoverable strain during stress controlled full transformation cycling in NiTi shape memory alloys. Scr Mater 2019;162:68–71.
[33] Zhao Zhihao, Xiao Yao, Lin Jianping, Min Junying. The roles of residual martensite and plastic deformation in thermomechanically coupled functional degradation of nanocrystalline superelastic NiTi alloys. J Mater Res Technol 2023;24:6791–807.
[34] Wan VVC, Cuddihy MA, Jiang J, MacLachlan DW, Dunne FPE. An HR-EBSD and computational crystal plasticity investigation of microstructural stress distributions and fatigue hotspots in polycrystalline copper. Acta Mater 2016;115:45–57.
[35] Chen Bo, Jiang Jun, Dunne Fionn PE. Is stored energy density the primary meso-scale mechanistic driver for fatigue crack nucleation? Int J Plast 2018;101:213–29.
[36] Bandyopadhyay Ritwik, Prithivirajan Veerappan, Peralta Alonso D, Sangid Michael D. Microstructure-sensitive critical plastic strain energy density criterion for fatigue life prediction across various loading regimes. Proc R Soc Lond Ser A Math Phys Eng Sci 2020;476(2236):20190766.
[37] Zhang Yahui, You Yajun, Moumni Ziad, Anlas Gunay, Zhu Jihong, Zhang Weihong. Stored-energy-based fatigue criterion for shape memory alloys. Smart Mater Struct 2019;28(6):065027.
[38] Schmahl Wolfgang W, Khalil-Allafi Jafar, Hasse B, Wagner M, Heckmann A, Somsen Ch. Investigation of the phase evolution in a super-elastic NiTi shape memory alloy (50.7 at.% Ni) under extensional load with synchrotron radiation. Mater Sci Eng A 2004;378(1–2):81–5.
[39] Carmine Maletta, Fabrizio Niccoli, Emanuele Sgambitterra, Franco Furgiuele. Analysis of fatigue damage in shape memory alloys by nanoindentation. Mater Sci Eng A 2017;684:335–43.
[40] Williamson GK, Hall WH. X-ray line broadening from filed aluminium and wolfram. Acta Metall 1953;1(1):22–31.
[41] Polatidis Efthymios, Zotov Nikolay, Bischoff Ewald, Mittemeijer Eric Jan. The effect of cyclic tensile loading on the stress-induced transformation mechanism in superelastic NiTi alloys: an in-situ X-ray diffraction study. Scr Mater 2015;100:59–62.
[42] Borbély András, Aoufi Asdin, Becht Dunstan. X-ray methods for strain energy evaluation of dislocated crystals. J Appl Crystallogr 2023;56(1).
[43] Faulkner EA. Calculation of stored energy from broadening of X-ray diffraction lines. Phil Mag 1960;5(53):519–21.